

Received 25 March 2025, accepted 16 April 2025, date of publication 24 April 2025, date of current version 6 May 2025.

Digital Object Identifier 10.1109/ACCESS.2025.3564237



Fabrication, Modeling, and Design of Position and Pressure Control System of a Soft **Pneumatic Linear Actuator**

LEANDRO SEITI GOIA, **DIEGO COLÓN**, AND ALEXANDRE BRINCALEPE CAMPO

Laboratory of Automation and Control, Universidade de São Paulo, São Paulo 05508-010, Brazil

Corresponding author: Leandro Seiti Goia (leandro.goia@usp.br)

This study was financed in part by the Coordenação de Aperfeiçoamento de Pessoal de Nível Superior - Brazil (CAPES) - Finance Code 001.

ABSTRACT The field of Soft Robotics proposes the use of flexible and compliant materials in the fabrication of soft actuators that can interact with humans in a safer way than conventional robots. While soft pneumatic actuators operate with positive pressure inflating their chambers and creating movement, vacuum actuators operate with negative pressure collapsing their chambers to generate movement. The latter have the benefit that they do not burst due to excessive pressure during contraction and since they shrink in size when activated, they can fit into tight spaces and are therefore more compact, aside from possibly being able to expand with positive pressure. This work presents a soft pneumatic linear actuator designed as a bellow-shaped structure made of silicone rubber that operates with negative pressure to contract and with positive pressure to extend. A Finite Element Method dynamic analysis was performed, using the SIMULIA Abaqus software, to predict the actuator's behavior. From the definition of the geometry, molds composed of modular pieces were designed and 3D printed to fabricate the actuator prototype. A test platform was designed to perform tests to characterize the actuator and then implement a position and pressure cascade control system, designed with a fuzzy pressure controller in the inner loop and a PI position controller in the outer loop, to regulate both the contraction and the extension of the actuator.

INDEX TERMS Soft Robotics, soft pneumatic actuator, finite element method, cascade control, graphical user interface.

I. INTRODUCTION

Soft actuators enable safer interaction between robots and humans and have applications in fields that can benefit from their mechanical characteristics. Robotic grippers made of soft bending actuators, such as the Pneunet, can grasp delicate and frail objects, which makes them useful in collaborative robots or in minimally invasive surgery, while soft linear actuators, such as the McKibben pneumatic artificial muscle (PAM), can be used in assistive devices [1].

In general, conventional robots are made up of rigid structures connected by joints and moved by electromechanical devices [2]. The inertia of the structure of industrial

The associate editor coordinating the review of this manuscript and approving it for publication was Hassen Ouakad.

robotic manipulators, for example, results in a possible danger to the environment in which they are in. Exoskeletons, which are devices that enhance the user's strength, endurance, and dexterity [3], are usually built in a similar way, which makes them capable of lifting heavy loads and supporting the user's body. However, their rigid structure is heavy, bulky and difficult to adapt to patients with different limb lengths, which might result in joint misalignment and discomfort [4]. Rehabilitation exoskeletons and orthoses should be compliant and lighter, to be more comfortable, adaptable [5] and biocompatible [6]. Therefore, the use of soft actuators has been seen as a possible solution to the aforementioned concerns.

Two of the most used soft pneumatic actuators are the Pneunet and McKibben pneumatic artificial muscle (PAM).

²Electrical Engineering Department, Instituto Federal de Educação, Ciência e Tecnologia de São Paulo, São Paulo 01109-010, Brazil



The first is comprised of a series of chambers made of silicone rubber that, when pressurized, inflate and bend due to the inextensible bottom layer [7]. It is used more commonly as a finger for soft robotic grippers to grasp more fragile and delicate bodies, but has also been used in robotic gloves for rehabilitation [8]. The second is a contractile actuator composed of an elastic tube inside a braided fiber wrapping that, when pressurized, inflates radially and contracts axially, due to the longitudinal constriction of the fibers [9]. It is usually used as an artificial muscle in upper and lower limb exoskeletons and in biomimetic continuum robots [10].

Alternatively, there are soft actuators that operate with negative pressure, in which their body collapses to generate a certain motion. Some benefits of this kind of operation are that the actuators cannot burst due to excessive pressure and their volume decreases during actuation, which makes them more compact and capable of fitting into narrower spaces [10]. In addition, they can also operate with positive pressures, that make them inflate and expand. Tawk et al. [11] proposed the Linear Soft Vacuum Actuator (LSOVA), 3D printed with thermoplastic polyurethane (TPU), with a cylindrical bellow-shaped structure, which collapses under negative pressure, generating motion in a straight line, which makes it an alternative to conventional linear actuators and to the McKibben PAM. Similarly, Oguntosin and Akindele [12] created the Soft Robotic Muscles (SRM), a prismatic actuator made of silicone rubbers of different hardness in the outer walls and inner chambers. Joe et al. [13], on the other hand, created the Ultralight Hybrid Pneumatic Artificial Muscle (UH-PAM), composed of a cylindrical bellow-shaped skin made of silicone rubber, with rigid inner rings and a foam backbone to prevent buckling during contraction.

The soft contractile actuators mentioned above can be used as artificial muscles in exoskeletons as pairs in antagonistic configuration, emulating the skeletal muscles of the human body, either by attaching their ends to straps around the limb [12] or to cables that rotate a pulley aligned with the wearer's joint [14]. They can also be used as linear actuators to pull tendons that are routed through the fingers of robotic grippers [15]. Multiple actuators can be used in a parallel configuration, in which their pulling force is summed when activated at the same time, while they can also be activated antagonistically to bend, acting as a continuum robotic arm [16]. Soft vacuum actuators, in particular, since they are more compact and act by shrinking, can be used as crawling robots to navigate inside tubes [17].

However, the downside of soft actuators is the complexity of their modeling and control, as they have complex geometries, their operation is based on continuum deformations, and the materials used to make them have nonlinear mechanical properties [2]. Initially, quasi-static models derived from free body diagrams can describe the interaction forces and deformations of the actuator [18]. A phenomenological dynamic model often used to represent McKibben PAMs is a three-element model consisting of a spring, a damping,

and an active contractile element [19]. As soft actuators have non-constant elasticity and damping, the model should include higher-order terms, approximated by polynomial expressions of the actuator's inner pressure [20].

An alternative is the Finite Element Method (FEM), a popular numerical tool that is capable of approximately simulating the behavior of soft actuators by calculating their displacement, stress tensions and output forces using hyperelastic constitutive models defined from experimental stress-strain test data [21]. A benefit of this technique is the ability to iteratively simulate and optimize the topology of soft robotic systems toward the desired behavior before their fabrication, preventing the potential waste of resources in experimental tests during the development of soft actuators.

Another commonly used technique is the parametric identification of soft actuator dynamic models [20] or closed box models [2] based on experimental data. It is well known that flexible systems can be modeled in this way [22], [23]. Since soft robots in general have nonlinear characteristics [24], convenient models are nonlinear autoregressive exogenous model (NARX) or Hammerstein-Wiener's model [25]. Algorithms for identification that could be used are regression algorithms, such as least squares methods, neural networks [26] or support vector machines [27].

In the initial stages of the design of a soft robot control system, the dynamic behavior may be analyzed based on experiments with an open-loop pressure control, with pumps and solenoid and pressure regulator valves [28], to identify certain operation parameters of the system, such as dead zones of pumps and valves, and saturation pressure of the actuators. From such data, it is possible to design a pressure feedback control system to regulate the pressure around setpoints within the operating range [29]. However, often the control variable of a soft robotic system is the position or force, making it necessary to design a cascade control system, with a pressure controller in the inner loop and a position or force controller in the outer loop [30]. In order to compensate for the nonlinearities of the soft actuators, the design should include nonlinear controllers. Some of the strategies found in the literature are adaptive Proportional-integral-derivative (PID) [31], [32], fuzzy [33], sliding-mode [26] and impedance control [14].

In this work, one designs position and pressure cascade control system for a soft pneumatic linear actuator, based on the LSOVA [11], but made of silicone rubber, like the SRM [12]. Initially, the geometry of the actuator was defined using FEM analysis. The molds for the fabrication of the soft actuator were designed and 3D printed. A 10-chamber prototype was characterized by means of experiments with different setpoint input signals on a platform with distance and pressure sensors. From the data analysis, the cascade control system was designed, with a fuzzy pressure controller and a PI position controller in the inner and outer loops, respectively. The control system was validated through step



response analysis to different setpoint values and through tests with the application of external loads.

A. PAPER'S ORIGINAL CONTRIBUTIONS

As long as the author's knowledge go, the paper presents several original contributions, which are pointed out in the following;

- 1) The development of an easy-to-use and low-cost technique to fabricate soft actuators with silicone rubber using molds composed of modular pieces;
- 2) The dynamic analysis of the FEM model of the proposed actuator;
- The design of a position and pressure cascade control system to regulate both the contraction and the extension of the actuator.

II. FINITE ELEMENT METHOD ANALYSIS

In order to define the actuator's geometry and analyze its dynamic behavior, a FEM analysis was performed, using Dassault Systèmes SIMULIA Abaqus for both the static and dynamic simulations. The actuator was modeled as an axisymmetric body with quadrilateral elements with eight nodes, with reduced integration and hybrid formulation (CAX8RH). The geometry of a single chamber actuator was based on the LSOVA's, but manually modified so as to have a similar behavior with a different material, with radius of 20mm, outer bellow-shaped walls with thickness of 2mm and 90-degree angle fold, top and bottom walls with thickness of 3mm, and a feeding hole with a diameter of 6mm, as shown in Fig. 1.

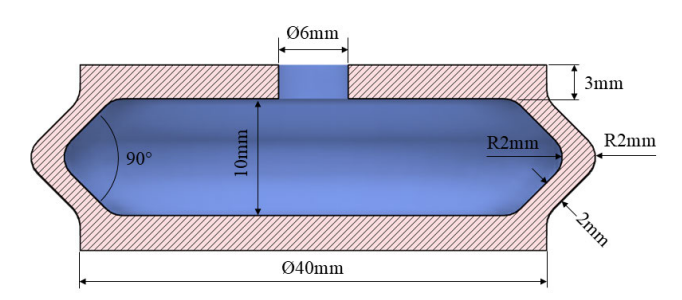


FIGURE 1. Geometry of the actuator's section.

The material chosen for the analysis was the Smooth-On Dragon Skin 20 silicone rubber. The model was defined as a material with density equal to $1.08g/cm^3$ and with the Yeoh hyperelastic constitutive material model, given by the strain energy density function W, defined in terms of the first invariant I_1 of the Cauchy-Green deformation tensor [34]:

$$W = C_{10}(I_1 - 3) + C_{20}(I_1 - 3)^2 + C_{30}(I_1 - 3)^3$$

The model coefficients presented in Table 1 were obtained from the stress-strain data extracted from the Soft Robotics Materials Database [35].

The boundary condition was defined as an encastre of the upper wall. The auto contact between the inner walls was

TABLE 1. Yeoh material model coefficients.

C_{10}	C_{20}	C_{30}	
0.1209	0.0011	0	

defined as tangential. The loads were defined as pressures on the inner walls. The actuator deformation was measured in the center node of the bottom wall. The initial static tests were performed with pressures of -4kPa, -3kPa, -2kPa, -1kPa, 2kPa, 4kPa, 6kPa and 8kPa. The resulting deformations are organized in Table 2. The actuator's final states are shown in Fig. 2. The pressure of -4kPa resulted in full contraction of the actuator, when the top and bottom walls of the chamber meet, with a displacement of 10.31mm, which is close to the chamber's height. On the other hand, the pressure of 8kPa resulted in a displacement of 6.05mm.

TABLE 2. Static deformations resultant of pressure steps.

Pressure (kPa)	Deformation (mm)
-4.0	10.31
-3.0	8.30
-2.0	5.68
-1.0	2.68
2.0	-2.76
4.0	-4.23
6.0	-5.25
8.0	-6.05

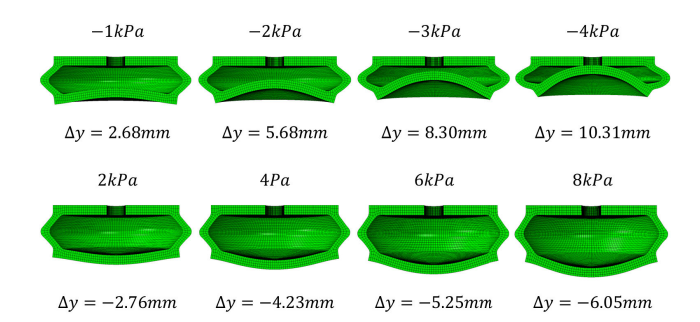


FIGURE 2. Deformations of the actuator in response to different pressures.

The dynamic analysis was performed through simulations with a period of 2.0 seconds, sample time 0.001 seconds and pressure steps applied at t=1.0 second. Analyzing the results, shown in Fig. 3 and Fig. 4, it is possible to note that the displacements are not proportional to the pressure loads and present different percentage overshoot, which points to nonlinear characteristics, since the gain and dampening of the system vary according to the load input.

A. MULTIPLE CHAMBERS

The geometry of the actuator with multiple chambers is illustrated by Fig. 5, with the section of a 2-chamber actuator. The walls separating each chamber, with a width of 3mm and an orifice of a diameter of 6mm, prevent radial deformations, prioritizing the axial deformation.

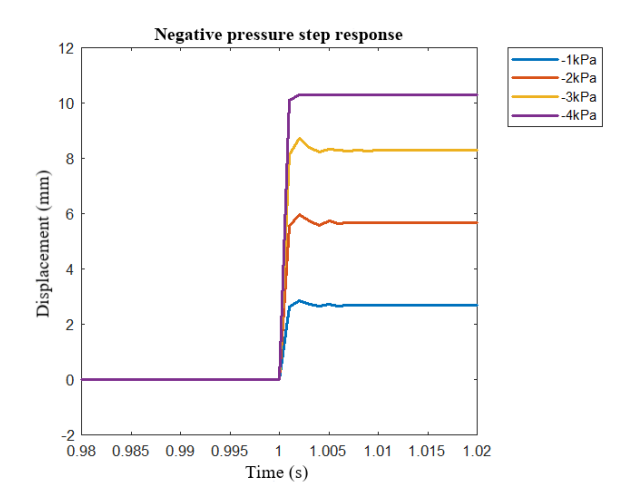


FIGURE 3. Negative pressure step responses.

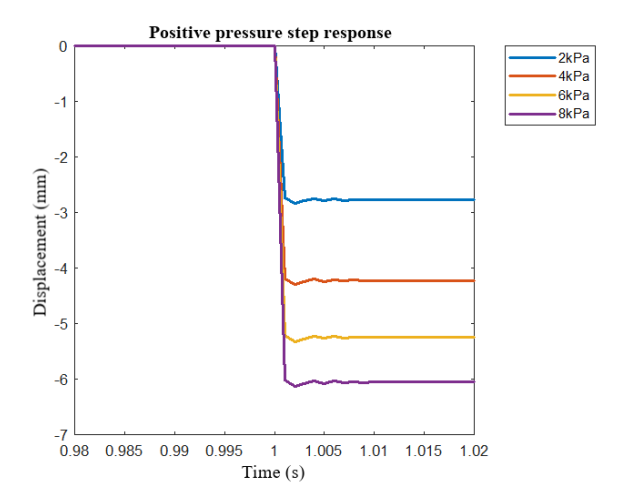


FIGURE 4. Positive pressure step responses.

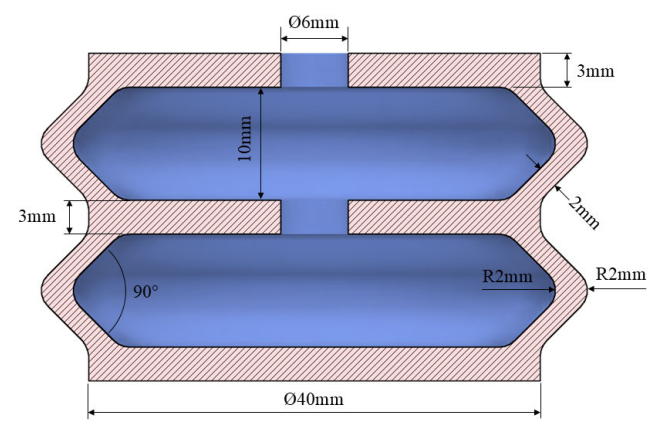


FIGURE 5. Dimensions of a 2-chamber actuator.

Based on the FEM analysis, it is reasonable to estimate that the full contraction deformations, when the top and bottom walls of each chamber touch each other, should be close to the number of chambers of the actuator times their height of 10mm.

III. FABRICATION

The actuator molds were designed in Autodesk Fusion 360 3D CAD software as modular pieces, as seen in Fig. 6, to facilitate assembly and disassembly in the molding process so that they can be stacked to mold prototypes with multiple chambers. The pieces were 3D printed with PLA.

The actuator fabrication is divided into two steps. Firstly, the silicone and catalyst mix, still liquid, is poured into the assembled mold. After the curing process, in a few hours, the mold is disassembled and then more silicone is poured into the brim molds to seal the extremities. Lastly, the fastener pieces are attached to the actuator brims, as shown in Fig. 7.

A prototype with two chambers was initially made using blue tin-based silicone rubber to validate the process. Then, two prototypes with four and eight chambers were made to verify the feasibility of longer series of chambers, as shown in Fig. 8. Subsequently, two prototypes with eight and ten chambers were fabricated with the Smooth-On Dragon Skin 20 silicone rubber, as shown in Fig. 9.

IV. TEST SETUP

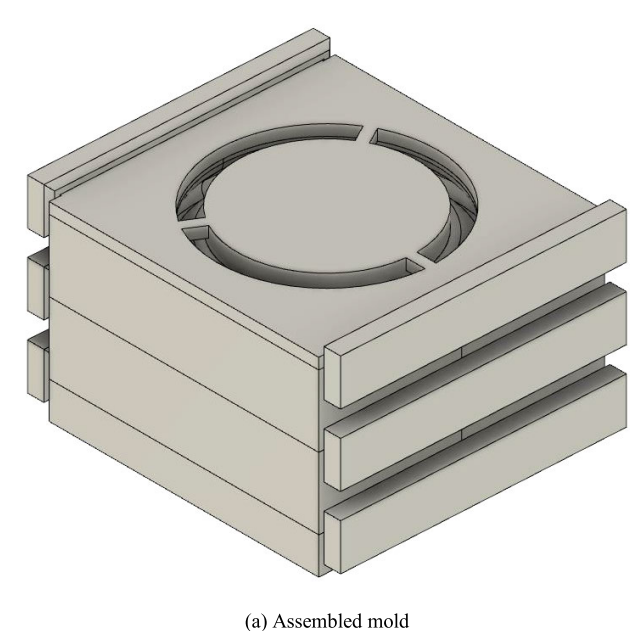
A test setup was designed to perform experimental characterization tests and implement the control system. The assembly is shown in Fig. 10. The structure is composed of $20 \times 20mm$ aluminum profiles. The actuator is attached to the top of the structure and a PVC pipe is used as a sliding rail attached to linear guides.

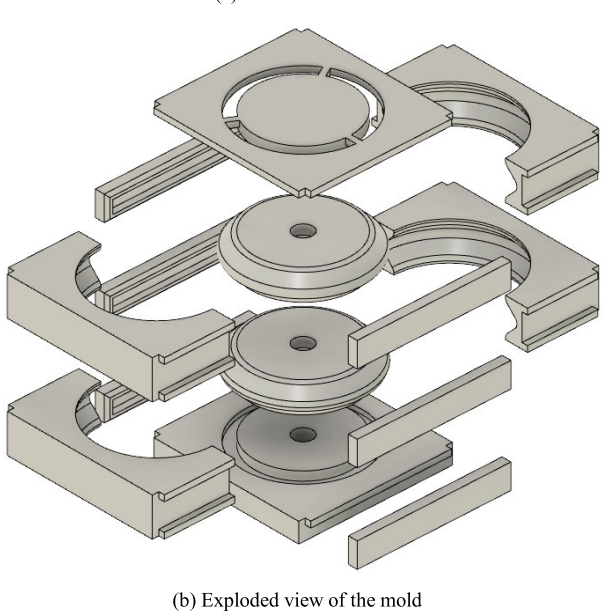
The diagram in Fig. 11 illustrates the operation of the setup. Through a graphical user interface (GUI), in MATLAB, the system parameters and the input signals are defined and sent, via a USB cable, to an Arduino Mega 2560 microcontroller, which sends the signals to the pneumatic system's drivers. The pneumatic system has two circuits: 1) one for positive pressures and 2) another for negative pressures. In the first, the pressure source is a Parker 12V D1001-23-01 pneumatic pump, the pressure is controlled by the SMC ITV1010 pressure regulator valve, and the circuit is switched by a 3/2-way solenoid valve. In the second, a pneumatic pump of the same model is used as a vacuum pump, connected directly to another solenoid valve. The pressure is measured by the NXP MPX10DP differential pressure sensor, and the displacement of the sliding rail is measured by a ST VL53L0X optical distance sensor.

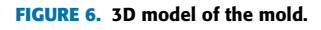
V. CHARACTERIZATION

In order to characterize the actuator, static tests were initially performed to measure the deformations of full contraction and extension of each prototype in response to negative and positive pressures, respectively, and the results were compared to the FEM model. In order to design the control system, dynamic step response tests were performed to analyze the system's transient response.









A. STATIC DEFORMATIONS ANALYSIS

Table 3 shows the deformations of the blue prototypes and Table 4 shows the results of the Dragon Skin ones. The registered deformations show that the full contractions result in deformations with more than double the displacement compared to the extensions. However, the prototypes might be capable of slightly greater extensions, since the pressure was not increased up to their rupture point.

Based on the height of the inner chamber, which is 10mm, and the deformation of a single chamber obtained in the FEM analysis, it was expected that the actuators would have

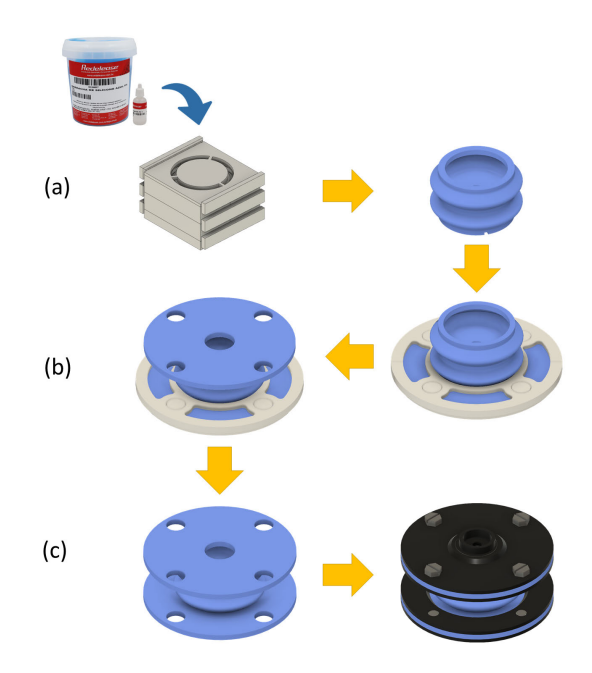
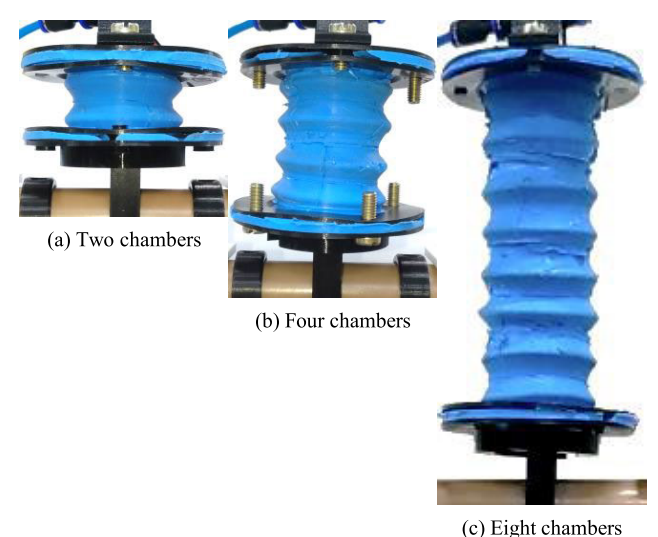


FIGURE 7. Fabrication process: (a) fabrication of the open body, (b) sealing of the extremities and the fastening brims, and (c) assembly of the fastening pieces.



(c) Eight chambers

full contractions proportional to the number of chambers, that is, deformations of 20mm, 40mm, 80mm and 100mm. However, the experimental measurements were smaller than those. The reason behind this might be the fact that the distance sensor measures the sliding rail displacement instead of the actuator's lower extremity, which was the reference point in the FEM analysis, and that the fastening pieces are rigid, limit the deformation of the upper and lower extremities of the actuator and increase its total weight, in addition to the possible irregularities in the inner walls due to air bubbles and impurities.

FIGURE 8. Prototypes made of the blue tin-based silicone rubber.



(b) Ten chambers

FIGURE 9. Prototypes made of Dragon Skin 20 silicone rubber.

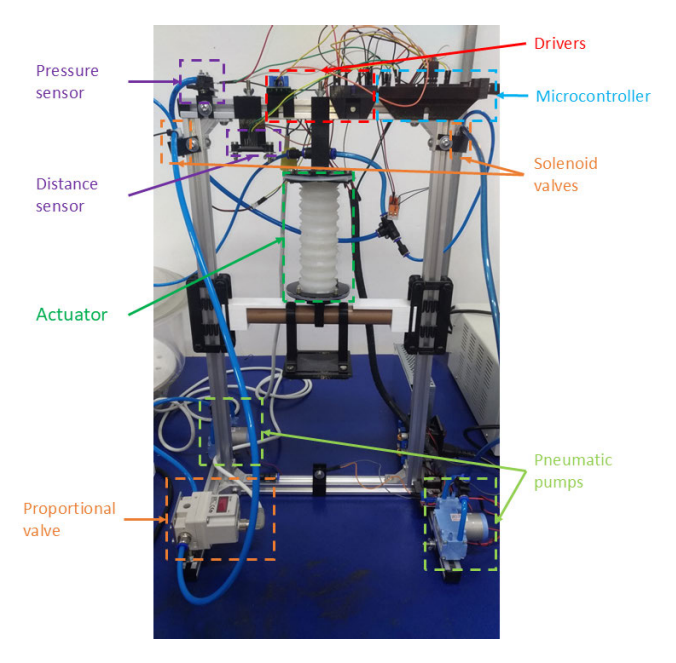


FIGURE 10. Test setup.

B. TRANSIENT RESPONSE ANALYSIS

In order to analyze the system's dynamics, tests were performed with the application of step signals of different amplitudes and the corresponding PWM duty cycle sent to the drivers. In the case of the negative pressure circuit, the signal is sent to the vacuum pump, whereas in the case of the positive pressure circuit, the signal is sent to the pressure

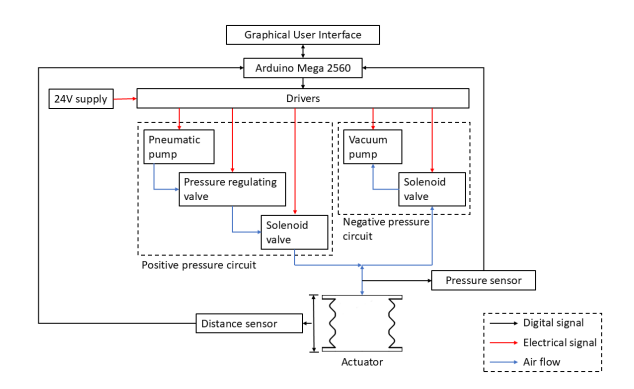


FIGURE 11. Setup operation diagram.

TABLE 3. Deformations of the blue prototypes.

Number of chambers	Contraction (mm)	Extension (mm)
2	12.3	6.0
4	26.7	12.2
8	60.6	28.6

TABLE 4. Deformations of the Dragon Skin 20 prototypes.

Number of chambers	Contraction (mm)	Extension (mm)		
8	64.8	32.2		
10	82.2	38.6		

regulator valve, while the pneumatic pump is maintained at 100%. In the initial tests, it was observed that the pumps and the pressure regulator valve have dead zones of up to 20% of PWM duty cycle. Therefore, step response tests were performed applying values from 30% to100%, with increments of 10%.

The graphs in Fig. 12 show that in response to steps applied to the vacuum pump's PWM signal, the pressure and distance decrease with fall time between 6s and 9s. However, the actuator resting state is not always the same, varying between 160mm and 170mm. The pressure saturation point is around 21.0kPa in response to signals over 70%. However, the actuator reaches full contraction, moving from the distance of 165mm to 84mm, under the pressure of around -15.0kPa, in response to the signal of 40% of PWM duty cycle. Some changes in inclination of the lines can be noted, possibly due to the saturation of each inner chamber, that do not happen at the same instant and make the actuator's body more rigid.

During positive pressure circuit tests, the pressure regulator valve was configured to maintain the pressure below 20kPa, preventing the actuator from rupture. The graphs in Fig. 13 show that in response to steps applied to the pressure regulator valve's PWM signal, the pressure and distance increase with rise time of 3s to 4s. The pressure and distance values seem close to proportional in response to signals of up to 80%, probably due to the pressure regulator valve's controller. The maximum distance measured was around 202mm, under pressure of around 18.5kPa, in response to signals over 90%.



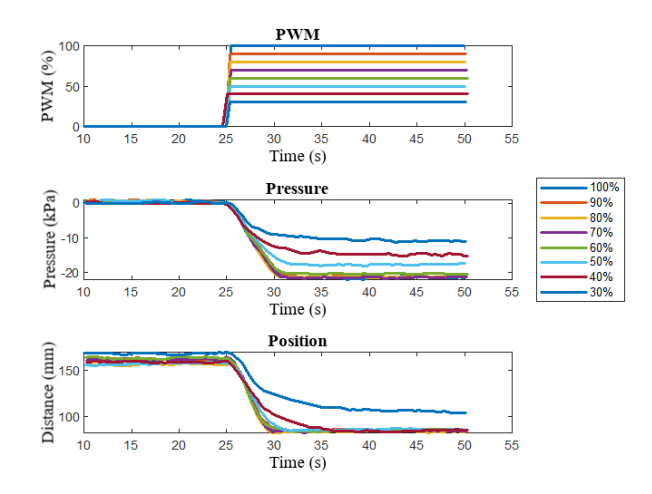


FIGURE 12. Step responses to vacuum pump's PWM steps.

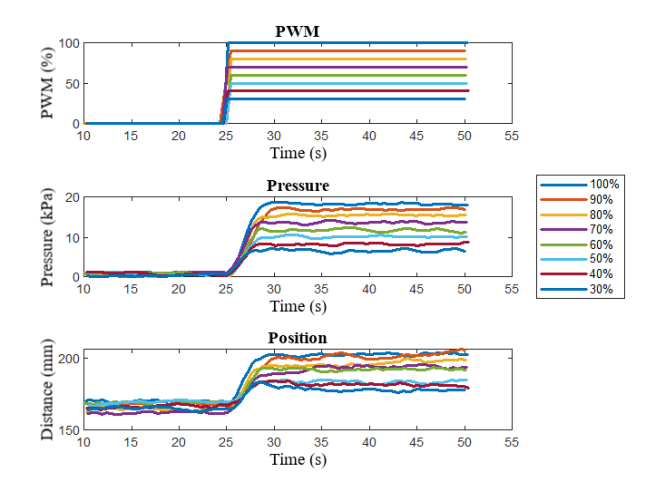


FIGURE 13. Step responses to pressure regulator valve's PWM steps.

VI. POSITION AND PRESSURE CASCADE CONTROL

Cascade control is a common approach used to achieve high-performance and high-robustness control systems [36]. It is common to use the inner loop to linearize the plant and the outer loop to give robustness to the system. A cascade control system was designed with the goal of controlling the actuator's position, both under contraction and extension, by regulating its inner pneumatic pressure, as illustrated in Fig. 14. The input is the position setpoint, defined by the user on the graphical user interface (GUI). In the outer position feedback loop, a proportional-integral (PI) controller generates the pressure setpoint, which is the input of the inner pressure feedback loop, in which a fuzzy controller regulates the control signal sent to the pressure regulator valve, for positive pressure, and to the vacuum pump, for negative pressure.

A. PRESSURE CONTROL SYSTEM

The inner loop is the pressure control system, which receives its setpoint from the outer loop position controller.

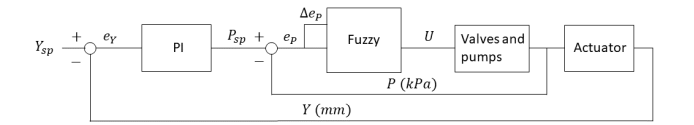


FIGURE 14. Block diagram of the position and pressure cascade control system.

1) FUZZY CONTROL

The pressure controller was designed as a fuzzy controller, with the pressure error e and the error change Δe as inputs, and changes in the PWM duty cycle Δu as output. Positive PWM values are sent to the pressure regulator valve, while the pneumatic pump PWM is kept at 100%, whereas the module of negative values is sent to the vacuum pump.

The membership functions were defined as triangular type. The fuzzy sets were named "Negative Big", "Negative Medium", "Negative Small", "Zero", "Positive Small", "Positive Medium" and "Positive Big", for all inputs and outputs. The inference rules were defined as shown in Table 5.

TABLE 5. Inference Rules for the fuzzy control.

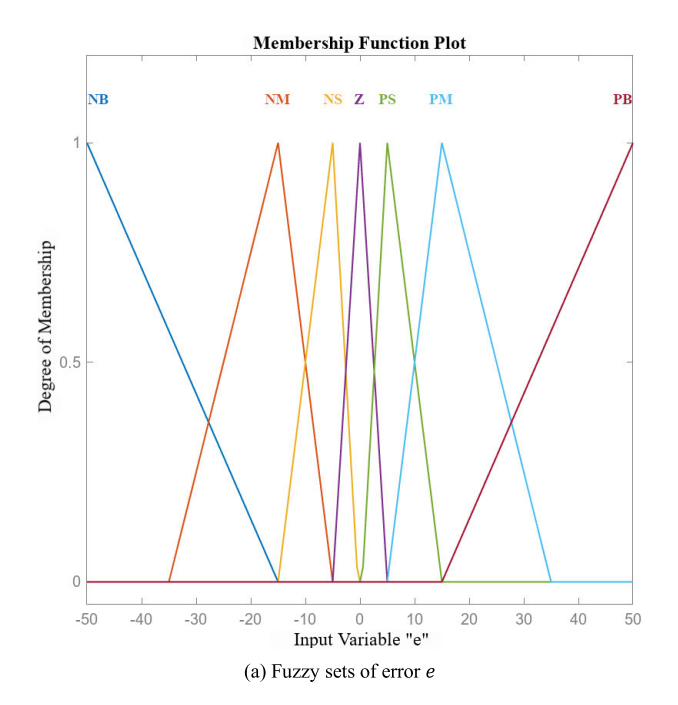
Δu		Δe						
	Δu	NB	NM	NS	Z	PS	PM	PB
	PB	Z	PS	PM	PB	PB	PB	PB
	PM	NS	Z	PS	PM	PB	PB	PB
	PS	NM	NS	Z	PS	PM	PB	PB
e	Z	NB	NM	NS	Z	PS	PM	PB
	NS	NB	NB	NM	NS	Z	PS	PM
	NM	NB	NB	NB	NM	NS	Z	PS
	NB	NB	NB	NB	NB	NM	NS	Z

Regarding the inputs, the minimum and maximum values were defined as -50kPa and 50kPa, as shown in Fig. 15, so as to cover the range from -25kPa up to 25kPa. For the output, the range was defined as -50% to 50% of PWM duty cycle, as shown in Fig. 16(a). The points of each set were experimentally tuned so as to make smaller changes when the pressure value is near the setpoint, avoiding overshoots, and bigger ones when it is far from it, resulting in the output surface shown in Fig. 16(b).

Since the behavior of the actuator under positive and negative pressures are different, two gains $K_p = 0.28$ (for positive) and $K_n = 0.068$ (for negative) were added to the system's output for manual fine tuning, as illustrated in Fig. 17, aiming at responses with overshoot under 10% of the setpoint.

2) RESULTS

The control system was validated by analyzing the step responses of different setpoint values, from -10kPa to -18kPa and from 10kPa to 18kPa. As seen in Fig. 18 and Fig. 19, it presented results according to the criteria, with overshoots and absolute error below 1kPa, therefore



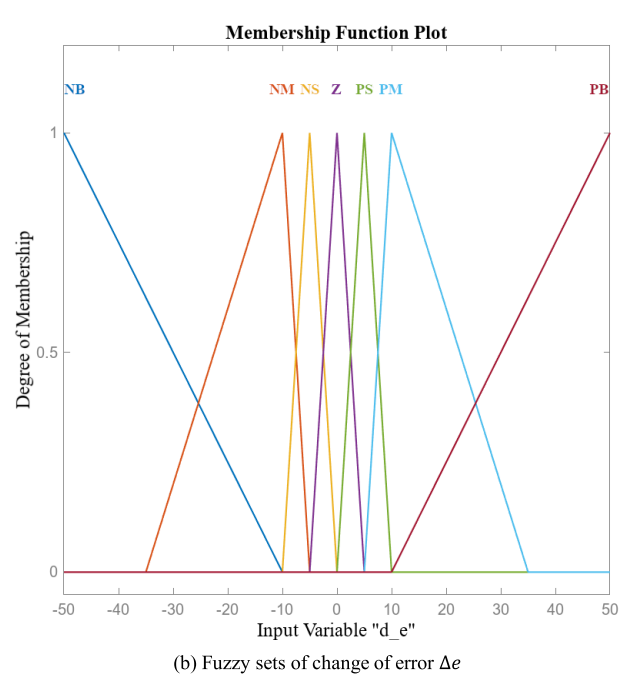


FIGURE 15. Input fuzzy sets.

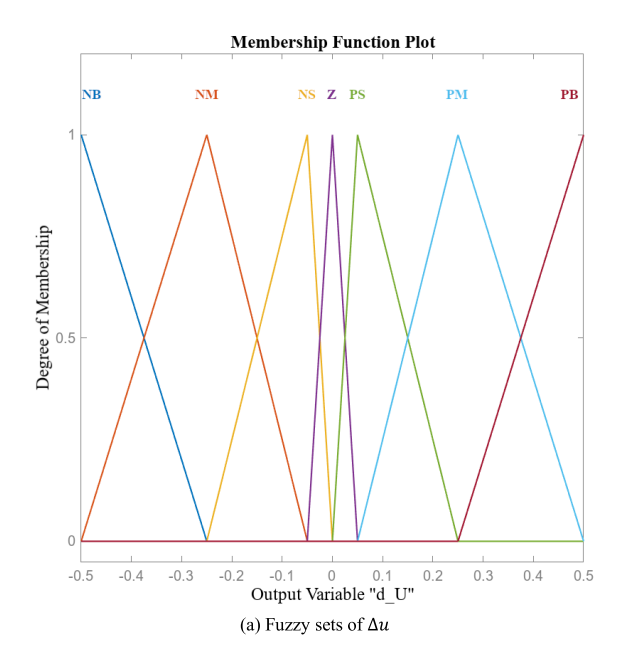
below 10% of the setpoint values. It is possible to note a delay of about 2.0 seconds due to the dead zones of the pressure regulator valve and the vacuum pump.

B. POSITION CONTROL

1) PROPORTIONAL-INTEGRAL CONTROL

The PI controller, in continuous time, can be given by:

$$u(t) = K_p e(t) + K_i \int_0^t e(t)dt$$



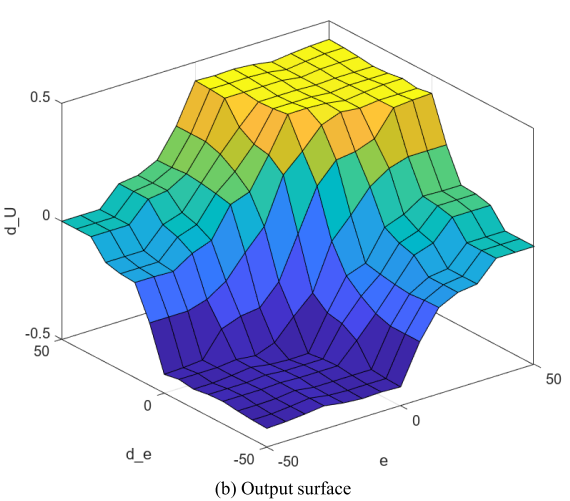
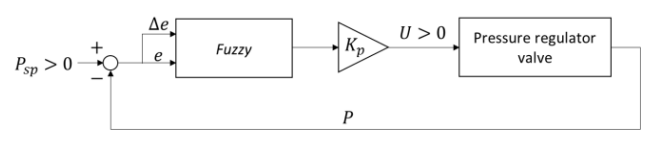
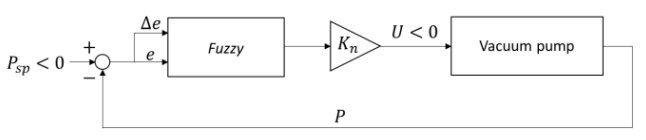


FIGURE 16. Output fuzzy sets and output surface.



(a) Positive pressure control diagram



(b) Negative pressure control diagram

FIGURE 17. Pressure control diagram.

By differentiating both sides and discretizing the derivatives by backward step, the controller becomes:

$$u(k) = u(k-1) + K_p(e(k) - e(k-1)) + K_i T_s e(k)$$



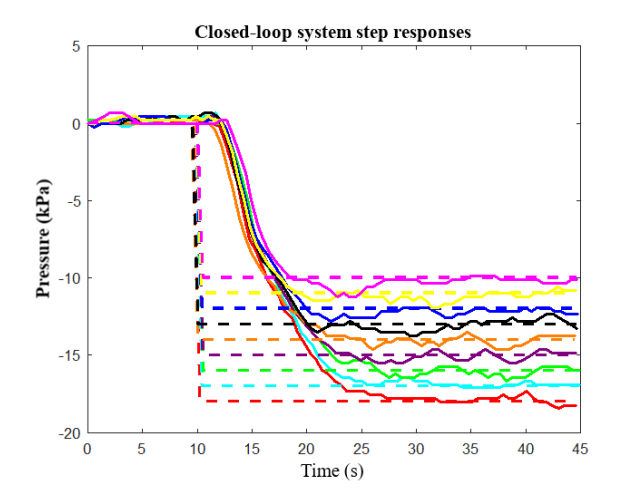


FIGURE 18. Closed-loop system step responses to negative pressures.

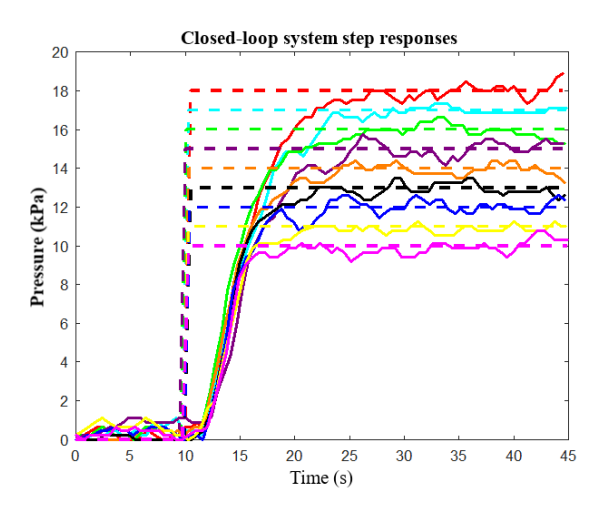


FIGURE 19. Closed-loop system step responses to positive pressures.

where T_s is the sampling time. Since the system behaves differently for negative and positive pressures, two PI controllers were designed, with the same structure, but with different proportional K_p and integral K_i gains. In order to design the position controller, a System Identification procedure for the pressure closed-loop control was performed, with the pressure setpoint as input and the position as the output. The identification data used were response signals to square waves of amplitude of 10kPa to 18kPa and of -10kPa to -15kPa, with steps of 1kPa and period of 50s. The validation data used were responses to step signals of the same amplitudes. The identifications were performed using MATLAB's System Identification Toolbox, to find ARX, ARMAX, Box-Jenkins and Output-Error models for each pressure amplitude [37].

The gains of the PI controller were then estimated for the models with highest fit rate, for each pressure amplitude, and the smaller ones were used as the controller's initial tuning, from which they were manually adjusted, aiming for step responses with overshoot below 10% of the setpoint value. The gains are shown in Table 6.

TABLE 6. PI controller gains.

	Negative	Pressure	Positive Pressure		
	Estimated Adjusted		Estimated	Adjusted	
K_p	0.0027	0.0018	0.0085	0.011	
K_i	0.0092	0.018	0.0282	0.057	

2) RESULTS

The position control system was validated by analyzing the step responses to setpoint values of -45mm, -55mm, -65mm and -75mm as negative positions and values of 20mm, 25mm, 30mm and 35mm as positive positions. The graphs in Fig. 20 (for negative positions) and Fig. 21 (for positive positions) show that the system presented results that satisfied the criteria of overshoot and absolute error below 10% of the setpoint value.

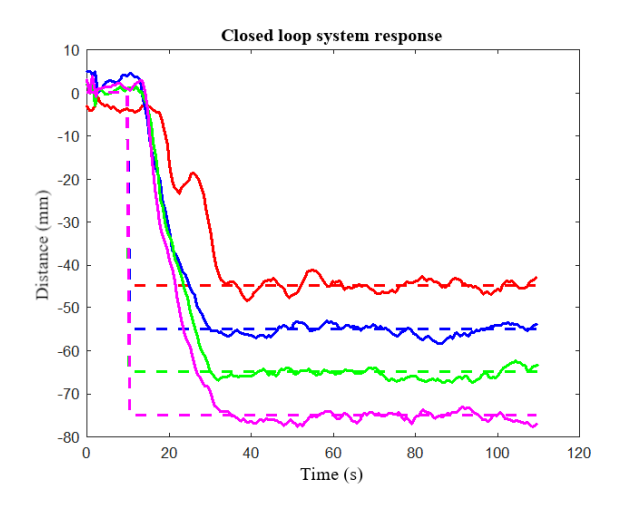


FIGURE 20. Closed-loop system step responses to negative positions.

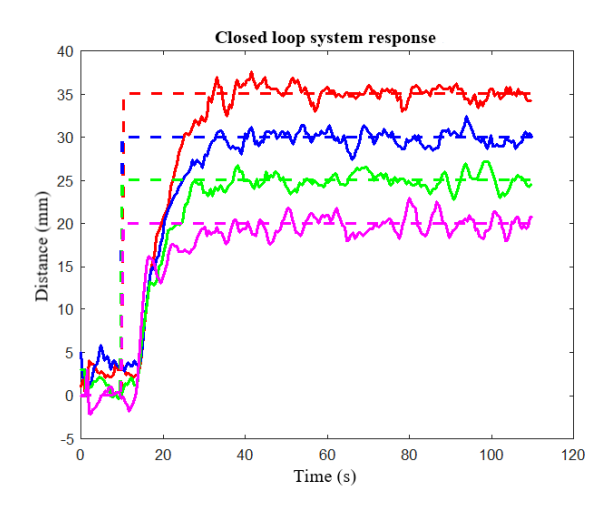


FIGURE 21. Closed-loop system step responses to positive positions.

3) EXTERNAL LOAD TEST

The disturbance rejection properties were tested by verifying the lifting capacity. Experiments were performed with



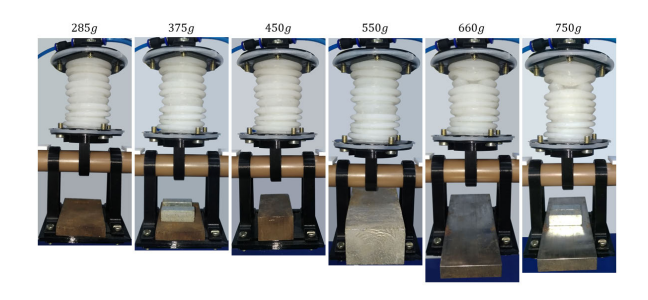


FIGURE 22. Lifting loads of 285q, 375q, 450q, 550q, 660q and 750q.

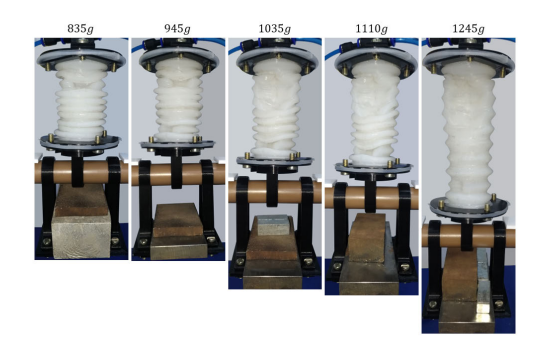


FIGURE 23. Lifting loads of 835g, 945g, 1035g, 1110g and 1245g.

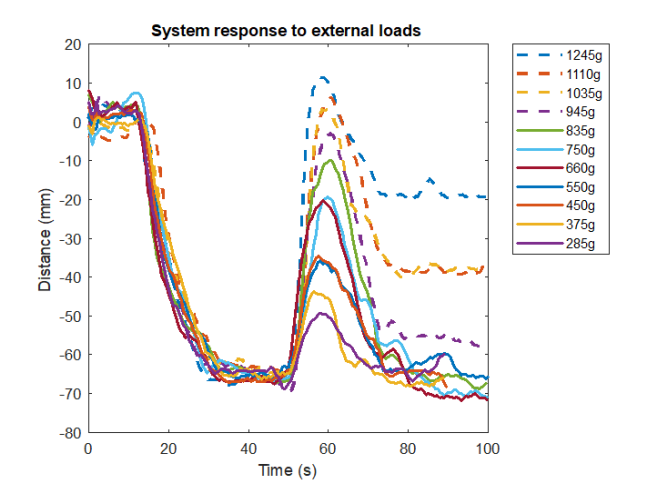


FIGURE 24. System response to external loads.

metallic weights of 285g, 375g, 450g, 550g, 660g, 750g, 835g, 945g, 1035g, 1110g and 1245g. The loads were manually added to a tray attached to the pipe. The position reference was defined as a step from the resting position of 0mm to the setpoint of -65mm, at t=10s. The weights were then loaded at t=50s. The final deformations of the actuator are shown in Fig. 22 and Fig. 23. It is possible to observe in the graphs in Fig. 24 that up to the load of 835g, the system was capable of returning to the position setpoint, which is expected in PI controllers. In the rest of the loads, some of the actuator's chambers collapsed radially, making it mechanically impossible for them to fold to reach the

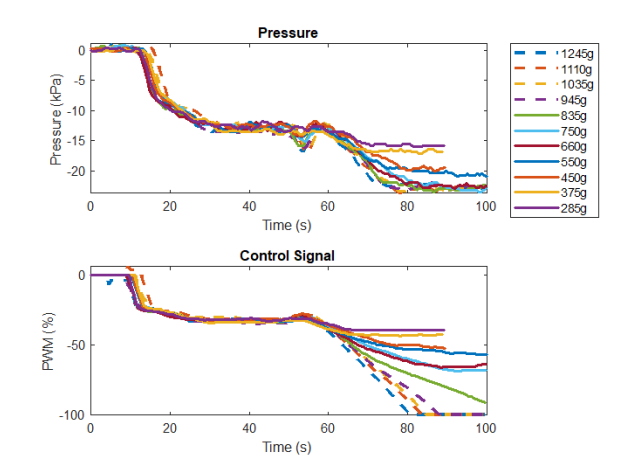


FIGURE 25. Pressure and control signals of the system response to external loads.

position setpoint, even with control signals of 100% of PWM, as shown in Fig. 25.

VII. CONCLUSION AND FUTURE WORKS

In this paper, a new low-cost design method for a complacent pneumatic contractile actuator is presented. Those actuators are based on models found in the literature and are made with silicone rubber. The innovation is in the molds, which are 3D printed and easily escalated to make larger actuators. Through the finite element method (FEM) analysis, the geometry could be modified to achieve a deformation of the actuator similar to the original model, but made of a different material and, therefore, with different mechanical properties. The FEM dynamic analysis shows that the actuator is nonlinear, that is, there is a gain variation to different pressure load inputs and saturation at full contraction or extension.

The 3D printed mold designed and the actuator's fabrication method proved to be practical and efficient, considering that it can be replicated several times to build prototypes with different number of chambers and, therefore, different lengths. In addition, the fastener pieces were designed so that they can be interchanged between different prototypes. A test setup was designed, in which the controllers are implemented in a graphical user interface (GUI) connected to a microcontroller, designed to make it possible to analyze the system's behavior in real time and process the data. Certain nonlinearities were noted, in addition to the ones seen in the FEM analysis, such as the dead zone of the pump and the pressure regulator valve at around 20% of PWM duty cycle.

A cascade closed-loop position control is developed, with the inner controller being a fuzzy controller for air pressure in the actuator, and the outer controller being a PI controller for position. The control systems presented reasonable results, with step responses with overshoot and absolute error below 10% of the setpoint signal, and were shown to be capable of reaching the desired position even with the addition of loads of up to 835g. The fuzzy controller provided nonlinearity compensation for the actuator PWM-position



functional relation. The PI controller was tuned based on transfer functions of the pressure-position functional relation (which is approximately linear and invariant in time) obtained by system identification techniques.

In future research, the actuator might be used in the design of an assistive device, such as an upper limb exoskeleton. In order to achieve the equipment's torque requirements, some modifications to the actuator design could be explored, such as different materials and the addition of rigid parts to increase its lifting capacity, rigidity and to prevent the radial collapse seen in the experiments with loads. Furthermore, repeatability tests may be conducted so as to evaluate the reliability and durability of the actuator. The pneumatic system could be modified, changing pumps and valves to ones with higher power and flow, to make the system stronger and faster and to decrease time delay.

Multiple actuators might be used together in a parallel configuration to achieve greater pulling strength when activated simultaneously or to bend when activated antagonistically, one with positive pressure and the other with negative pressure, making up a system with more degrees of freedom in addition to the linear motion of a single actuator. Furthermore, a fault-tolerant control system could be implemented so that if an actuator ruptures, the controller could isolate it and compensate by increasing the effort of another one in parallel, in an attempt to keep the device working or to shut it down safely without an abrupt movement or a sudden stop.

ACKNOWLEDGMENT

Leandro Seiti Goia thanks CAPES (Brazilian agency for graduate studies) for the master's scholarship, the Federal Institute of São Paulo (IFSP) for allowing the use of the Laboratory of Applied Control, and the students Rafael dos Santos Souza da Cruz and Maylon Rodrigues Nunes dos Santos for the support during the development of the project.

REFERENCES

- J.-H. Hsiao, J.-Y. Chang, and C.-M. Cheng, "Soft medical robotics: Clinical and biomedical applications, challenges, and future directions," *Adv. Robot.*, vol. 33, no. 21, pp. 1099–1111, Nov. 2019.
- [2] A. Das and M. Nabi, "A review on soft robotics: Modeling, control and applications in human-robot interaction," in *Proc. Int. Conf. Comput.*, *Commun.*, *Intell. Syst. (ICCCIS)*, Oct. 2019, pp. 306–311.
- [3] N. Aliman, R. Ramli, and S. M. Haris, "Design and development of lower limb exoskeletons: A survey," *Robot. Auto. Syst.*, vol. 95, pp. 102–116, Sep. 2017. [Online]. Available: https://www.sciencedirect.com/science/ article/pii/S0921889016304274
- [4] Mae. Irshaidat, M. Soufian, A. Elkurdi, and S. Nefti-Meziani, "Soft and hard robotics for movement rehabilitation, analysis and modelling," in *Proc. 12th Int. Conf. Develop. eSystems Eng. (DeSE)*, Oct. 2019, pp. 964–969.
- [5] A. J. Veale and S. Q. Xie, "Towards compliant and wearable robotic orthoses: A review of current and emerging actuator technologies," *Med. Eng. Phys.*, vol. 38, no. 4, pp. 317–325, Apr. 2016. [Online]. Available: https://www.sciencedirect.com/science/article/pii/S135045331600031X
- [6] S. de Siqueira Rodrigues Fleury Rosa, M. do Carmo Reis, M. F. F. Rosa, D. Colón, C. A. dos Reis, and J. M. Balthazar, "Use of natural latex as a biomaterial for the treatment of diabetic foot a new approach to treating symptoms of diabetes mellitus," in *Topics in Public Health*, D. Claborn, Ed., Rijeka, Croatia: IntechOpen, 2015, ch. 10.

- [7] B. Mosadegh, P. Polygerinos, C. Keplinger, S. Wennstedt, R. F. Shepherd, U. Gupta, J. Shim, K. Bertoldi, C. J. Walsh, and G. M. Whitesides, "Soft robotics: Pneumatic networks for soft robotics that actuate rapidly (Adv. Funct. Mater. 15/2014)," Adv. Funct. Mater., vol. 24, no. 15, p. 2109, Apr. 2014
- [8] P. Polygerinos, S. Lyne, Z. Wang, L. F. Nicolini, B. Mosadegh, G. M. Whitesides, and C. J. Walsh, "Towards a soft pneumatic glove for hand rehabilitation," in *Proc. IEEE/RSJ Int. Conf. Intell. Robots Syst.*, Nov. 2013, pp. 1512–1517.
- [9] Q. Liu, J. Zuo, C. Zhu, and S. Q. Xie, "Design and control of soft rehabilitation robots actuated by pneumatic muscles: State of the art," *Future Gener. Comput. Syst.*, vol. 113, pp. 620–634, Dec. 2020. [Online]. Available: https://www.sciencedirect.com/science/article/pii/S0167739X20306543
- [10] A. Pagoli, F. Chapelle, J.-A. Corrales-Ramon, Y. Mezouar, and Y. Lapusta, "Review of soft fluidic actuators: Classification and materials modeling analysis," *Smart Mater. Struct.*, vol. 31, no. 1, Jan. 2022, Art. no. 013001.
- [11] C. Tawk, G. M. Spinks, M. in het Panhuis, and G. Alici, "3D printable linear soft vacuum actuators: Their modeling, performance quantification and application in soft robotic systems," *IEEE/ASME Trans. Mechatronics*, vol. 24, no. 5, pp. 2118–2129, Oct. 2019.
- [12] V. Oguntosin and A. Akindele, "Design and characterization of artificial muscles from wedge-like pneumatic soft modules," Sens. Actuators A, Phys., vol. 297, Oct. 2019, Art. no. 111523. [Online]. Available: https:// www.sciencedirect.com/science/article/pii/S0924424719309884
- [13] S. Joe, H. Wang, M. Totaro, and L. Beccai, "Development of ultralight hybrid pneumatic artificial muscle for large contraction and high payload," in *Proc. 3rd IEEE Int. Conf. Soft Robot. (RoboSoft)*, May 2020, pp. 27–32.
- [14] Q. Liu, Y. Liu, C. Zhu, X. Guo, W. Meng, Q. Ai, and J. Hu, "Design and control of a reconfigurable upper limb rehabilitation exoskeleton with soft modular joints," *IEEE Access*, vol. 9, pp. 166815–166824, 2021.
- [15] C. Tawk, A. Gillett, M. in het Panhuis, G. M. Spinks, and G. Alici, "A 3D-printed omni-purpose soft gripper," *IEEE Trans. Robot.*, vol. 35, no. 5, pp. 1268–1275, Oct. 2019.
- [16] X. Li, T. Zheng, D. Sui, N. Lin, Q. Zhang, J. Zhao, and Y. Zhu, "A 3D printed variable cross-section pneumatic soft manipulator with high-precision positioning capability: Design and control implementation," Sens. Actuators A, Phys., vol. 342, Aug. 2022, Art. no. 113644. [Online]. Available: https://www.sciencedirect.com/science/article/pii/S0924424722002825
- [17] M. S. Verma, A. Ainla, D. Yang, D. Harburg, and G. M. Whitesides, "A soft tube-climbing robot," *Soft Robot.*, vol. 5, no. 2, pp. 133–137, Apr. 2018.
- [18] C. T. O'Neill, N. S. Phipps, L. Cappello, S. Paganoni, and C. J. Walsh, "A soft wearable robot for the shoulder: Design, characterization, and preliminary testing," in *Proc. Int. Conf. Rehabil. Robot. (ICORR)*, Jul. 2017, pp. 1672–1678.
- [19] D. B. Reynolds, D. W. Repperger, C. A. Phillips, and G. Bandry, "Modeling the dynamic characteristics of pneumatic muscle," *Ann. Biomed. Eng.*, vol. 31, no. 3, pp. 310–317, Mar. 2003.
- [20] D. Zhang, X. Zhao, and J. Han, "Active modeling for pneumatic artificial muscle," in *Proc. IEEE 14th Int. Workshop Adv. Motion Control (AMC)*, Apr. 2016, pp. 44–50.
- [21] C. Tawk and G. Alici, "Finite element modeling in the design process of 3D printed pneumatic soft actuators and sensors," *Robotics*, vol. 9, no. 3, p. 52, Jul. 2020. [Online]. Available: https://www.mdpi.com/2218-6581/ 9/3/52
- [22] A. A. Felix, D. Colón, B. M. Verona, L. W. S. L. Ramos, H. Cobas-Gomez, and M. R. Gongora-Rubio, "Modeling, identification and controller design for an electrostatic microgripper," in *Mechanisms and Machine Science*, J. M. Balthazar, Ed., Cham, Switzerland: Springer, 2021, pp. 317–331.
- [23] A. A. Felix, D. Colón, B. M. Verona, L. W. S. L. Ramos, H. Cobas-Gomez, and M. R. Gongora-Rubio, "Identification and robust controllers for an electrostatic microgripper," *J. Vibrat. Eng. Technol.*, vol. 9, no. 3, pp. 389–397, Apr. 2021, doi: 10.1007/ s42417-020-00241-2.
- [24] D. Colón, Á. M. Bueno, Y. S. Andrade, I. S. Diniz, and J. M. Balthazar, "Nonlinear ball and beam control system identification," *Appl. Mech. Mater.*, vol. 706, pp. 69–80, Dec. 2014.
- [25] D. Bruder, C. D. Remy, and R. Vasudevan, "Nonlinear system identification of soft robot dynamics using Koopman operator theory," in *Proc. Int. Conf. Robot. Autom. (ICRA)*, May 2019, pp. 6244–6250.



- [26] Q. Liu, Y. Liu, Y. Li, C. Zhu, W. Meng, Q. Ai, and S. Q. Xie, "Path planning and impedance control of a soft modular exoskeleton for coordinated upper limb rehabilitation," Frontiers Neurorobotics, vol. 15, pp. 1–12, Nov. 2021. [Online]. Available: https://www.frontiersin.org/ journals/neurorobotics/articles/10.3389/fnbot.2021.745531
- [27] H. Liu, J. Tao, P. Lyu, and F. Tian, "Human-robot cooperative control based on sEMG for the upper limb exoskeleton robot," *Robot. Auto. Syst.*, vol. 125, Mar. 2020, Art. no. 103350. [Online]. Available: https://www.sciencedirect.com/science/article/pii/S0921889018307462
- [28] A.-F. Hassanin, D. Steve, and N.-M. Samia, "A novel, soft, bending actuator for use in power assist and rehabilitation exoskeletons," in *Proc. IEEE/RSJ Int. Conf. Intell. Robots Syst. (IROS)*, Sep. 2017, pp. 533–538.
- [29] F. Wang, H. Wang, J. Luo, X. Kang, X. Zhang, L. Chen, and Q. Pan, "Design and research of a soft hand rehabilitation robot with multiple training modes," in *Proc. 3rd Int. Conf. Comput.*, *Netw. Internet Things* (CNIOT), May 2022, pp. 171–175.
- [30] L. S. Goia, A. B. Campo, and D. Colón, "Modelling, control and applications of soft pneumatic actuators in upper-limb exoskeletons: A systematic review," in *Proc. Latin Amer. Robot. Symp. (LARS)*, *Brazilian Symp. Robot. (SBR), Workshop Robot. Educ. (WRE)*, Oct. 2022, pp. 1–6.
- [31] M. Haghshenas-Jaryani, C. Pande, and M. Wijesundra, "Soft robotic bilateral hand rehabilitation system for fine motor learning," in *Proc. IEEE* 16th Int. Conf. Rehabil. Robot. (ICORR), Jun. 2019, pp. 337–342.
- [32] P. U. M. Liduário, D. Colón, Á. M. Bueno, E. P. Godoy, and J. M. Balthazar, "Identification and practical control of a fluid plant," in *Proc. ABCM Symp. Ser. Mechatronics*, vol. 6, 2014, pp. 1095–1104.
- [33] H. Al-Fahaam, S. Davis, S. Nefti-Meziani, and T. Theodoridis, "Novel soft bending actuator-based power augmentation hand exoskeleton controlled by human intention," *Intell. Service Robot.*, vol. 11, no. 3, pp. 247–268, Jul. 2018.
- [34] X. Li and Y. Wei, "Classic strain energy functions and constitutive tests of rubber-like materials," *Rubber Chem. Technol.*, vol. 88, no. 4, pp. 604–627, Dec. 2015, doi: 10.5254/rct.15.84879.
- [35] L. Marechal, P. Balland, L. Lindenroth, F. Petrou, C. Kontovounisios, and F. Bello, "Toward a common framework and database of materials for soft robotics," *Soft Robot.*, vol. 8, no. 3, pp. 284–297, Jun. 2021.
- [36] C. A. dos Reis, H. D. O. Florentino, D. Cólon, S. R. F. Rosa, and D. R. Cantane, "An approach of the exact linearization techniques to analysis of population dynamics of the mosquito aedes aegypti," *Math. Biosciences*, vol. 299, pp. 51–57, May 2018.
- [37] L. Ljung, System Identification: Theory for the User (PTR Prentice-Hall Information and System Science Series), 2nd ed., Upper Saddle River, NJ, USA: Prentice-Hall, 1999.



LEANDRO SEITI GOIA received the B.S. degree in control and automation engineering from Instituto Federal de Educação, Ciência e Tecnologia de São Paulo (IFSP), in 2020, and the M.S. degree in systems engineering from the Polytechnic School, Universidade de São Paulo, in 2024, where he is currently pursuing the Ph.D. degree.



DIEGO COLÓN received the B.S. degree in electrical engineering, and the M.S. and Ph.D. degrees in systems engineering from the Polytechnic School, University of São Paulo, Brazil, in 1997, 1999, and 2003, respectively. He is currently a Consultant with the National Council for Scientific and Technological Development, a Consultant with the Foundation for Research Support of the State of São Paulo (FAPESP), and an Associate Professor with the Polytechnic

School, Universidade de São Paulo. He has experience in electrical engineering, acting on the following subjects: control systems, industrial automation, adaptive control, discrete control, and nonlinear control.



ALEXANDRE BRINCALEPE CAMPO received the B.S. degree in electrical engineering, and the M.S. and Ph.D. degrees in systems engineering from the Polytechnic School, University of São Paulo, Brazil, in 1991, 1995, and 2001, respectively. In 2014, he was hosted as a Visiting Professor with Harvard University, USA. He is currently a Full Professor with Instituto Federal de Educação, Ciência e Tecnologia de São Paulo (IFSP), where he is responsible for subjects in

the control area of the control and automation engineering and electronic engineering course. He is the Coordinator of the IFSP's Applied Control Laboratory (LCA), with patents filed and granted, and one of them is licensed to Soft Grippers Company, of which he is a Shareholder. His research interests include soft robotics and control of magnetic levitation systems (MAGLEV).

• • •